Available online at www.sciencedirect.com
SCIENCE DIRECT®
International Journal of Thermal Sciences 43 (2004) 241–247
International Journal of Thermal Sciences
www.elsevier.com/locate/ijts

Three-dimensional numerical simulation of an array of impinging laminar square jets with spent fluid removal

L.B.Y. Aldabbagh, I. Sezai *

Mechanical Engineering Department, Eastern Mediterranean University, Magosa, Mersin 10, Turkey

Received 16 July 2002; received in revised form 16 June 2003; accepted 17 June 2003

Abstract

A three-dimensional numerical study is used to investigate the heat transfer characteristics of a 3×3 array of square jets with spent fluid removal through holes placed between nozzles on the confinement plate. The influence of the jet-to-jet spacing and nozzle to plate spacing is considered for different Reynolds numbers in the laminar range. For very small nozzle-to-plate distances ($L_z \approx 0.25D$), spent fluid removal lowers the local Nusselt number in localities below the spent air holes as a result of detachment of the wall jets as the fluid is directed away from the impingement plate towards the spent air holes. Spent fluid removal increased the heat transfer rate for a larger nozzle to plate spacing of $2D$ for jet-to-jet spacings less than $4D$. The effect of spent fluid removal is higher for smaller jet-to-jet spacings due to more intense jet interactions and cross flow effects.

Keywords: Jet arrays; Spent fluid removal

1. Introduction

Impinging jets have found a large number of applications where high rates of convective heat transfer are required. Industrial uses of impinging air jets include tempering of glass, drying of paper and textiles, and the cooling of the metal sheets, micro-electronic components and turbine blades. Although such jets yield very high heat transfer coefficients in the stagnation zone the cooling performance drops rapidly away from the impingement zone. For this reason, and to increase the uniformity of the heat flux distribution, jets are often used in arrays. In addition, arrays of jets are used when heating or cooling a variety of industrial products with large surface areas. In such cases the interaction between the crossflow and the adjacent jets heavily influences the heat transfer performance of the individual jets in the array. As a result, drainage of the spent fluid is a critical issue in jet array applications. Studies with arrays of jets (Florschuetz et al. [1], Obot and Trabold [2], Garrett and Webb [3]) have shown that crossflow, caused by the spent fluid exiting radially outward, decreases the heat transfer associated with the impinging jets and results in nonuniform distribution of heat transfer coefficient. Crossflow effects can be minimized by having the spent air exit through vent holes either placed in the impingement plate or in the orifice plate between the jet nozzles.

Studies on spent fluid removal through vent holes in jet array systems are rather scarce. Hollworth and Dagan [4] examined experimentally an impinging jet array system with spent fluid exits distributed on the impingement surface, disclosing that for arrays with staggered spent air exit holes, the heat transfer rate is 20–30% higher than that without spent fluid removal. Huber and Viskanta [5] experimentally investigated the effect of placing spent air exits located between the jet orifices in the jet orifice plate on the local Nusselt number distributions for axisymmetric confined air jet arrays in the turbulent regime.

The only known numerical work on spent fluid removal through vent exits placed between the jet arrays on the orifice plate belongs to Tzeng et al. [6]. They found that overall heat transfer performance increases as the spent fluid suction rate increased.

Although many applications involve turbulent jets, laminar jets are also encountered when the fluid is viscous (e.g., liquid) or the geometry is miniature as in microelectronics. Moreover, numerical simulations of impinging jets us-

* Corresponding author.
E-mail address: ibrahim.sezai@emu.edu.tr (I. Sezai).

1290-0729/$ – see front matter
doi:10.1016/j.ijthermalsci.2003.06.003

Nomenclature

A_x, A_y, A_z	aspect ratios in x-, y- and z-direction, $= L_x/D$, $= L_y/D$, $= L_z/D$
D	jet width ..... m
Gr	Grashof number
h	heat transfer coefficient ..... $W{\cdot}m^{-2}{\cdot}K^{-1}$
k	thermal conductivity ..... $W{\cdot}m^{-1}{\cdot}K^{-1}$
L_x, L_y, L_z	length of heated surface in x-, y- and z-directions, respectively ..... m
Nu	local Nusselt number, $= hD/k$
P	nondimensional pressure, $= p/\rho u_j^2$
p	pressure ..... $N{\cdot}m^{-2}$
Pr	Prandtl number, $= \nu/\alpha$
q''_w	local convective heat flux at the impingement plate ..... $W{\cdot}m^{-2}$
Re	jet Reynolds number, $= u_j D/\nu$
T	nondimensional temperature, $= (t - t_j)/(t_w - t_j)$
t	temperature ..... °C
u_j	jet exit velocity ..... $m{\cdot}s^{-1}$
U	nondimensional Cartesian velocity, in x-direction, $= u/u_j$
V	nondimensional Cartesian velocity, in y-direction, $= v/u_j$
W	nondimensional Cartesian velocity, in z-direction, $= w/u_j$
u, v, w	Cartesian velocities ..... $m{\cdot}s^{-1}$
x_n	jet-to-jet spacing ..... m
X_n	jet–jet spacing/jet width ratio, $= x_n/D$
X, Y, Z	nondimensional Cartesian coordinates, $= x/D$, $= y/D$, $= z/D$, respectively
x, y, z	Cartesian coordinates

Greek symbols

ν	kinematic viscosity ..... $m^2{\cdot}s^{-1}$
ρ	density ..... $kg{\cdot}m^{-3}$
α	thermal diffusivity ..... $m^2{\cdot}s^{-1}$
ϕ	U, V, W, P, or T field

Subscripts

j	jet exit
w	wall

ing different turbulence models lack generality owing to the absence of a very wide range of scales in the models. Hence, we use computations in the laminar range in order to obtain the complex flow structures encountered in jet array system. The numerical simulation of jet array system in the laminar range is also quite scarce. The numerical simulations of Mikhail et al. [7], Seyedein et al. [8] and Laschefski et al. [9] are related with impingement of rows of laminar slot jets which are all two-dimensional. The present work deals with laminar, three-dimensional, analysis of 3×3 square array of confined square air jets impinging on a heated flat surface with spent fluid removal. A detailed picture of the flow field is obtained and used to understand the local variation of the Nusselt number in the array.

2. Computation scheme

In an array, jets are usually arranged in parallel rows. For this study a 3×3 square jet array system is used. The center jet is completely surrounded by adjacent jets, similar to an individual jet in an array. Spent air exit holes are placed between the jet nozzles on the nozzle plate as shown in Fig. 1. Both the jet nozzles and spent fluid exit nozzles have square cross section of dimensions D. The hatched area is the total impingement surface area cooled by the center jet. This is similar to the "unit cell" defined in the experimental study of Huber and Viskanta [5]. The center jet represents an individual jet in the array in the absence of cross flow. This is true if the mass flow rate at spent fluid exit is equal to mass flow rate at jet exit. In that case the average heat transfer coefficient calculated on the area defied by the unit cell represents the average convection heat transfer coefficient of the entire jet array system.

The steady-state, three-dimensional, Navier–Stokes and energy equations for incompressible flows in Cartesian coordinates are used for this study. The velocity and length are nondimensionalized by jet-exit velocity and jet width, respectively. The buoyancy effect has been neglected. It is known that for Gr/Re^2 in the order of unity or above the buoyancy effect cannot be neglected. However, as a first analysis and to separate the effect of different parameters it is decided to neglect buoyancy. Hence the analysis is valid for $Gr/Re^2 \ll 1$.

The nondimensional continuity, momentum and energy equations for laminar flow with constant properties can be written as:

$$\frac{\partial U}{\partial X} + \frac{\partial V}{\partial Y} + \frac{\partial W}{\partial Z} = 0 \tag{1}$$

$$U\frac{\partial U}{\partial X} + V\frac{\partial U}{\partial Y} + W\frac{\partial U}{\partial Z} = -\frac{\partial P}{\partial X} + \frac{1}{Re}\nabla^2 U \tag{2}$$

$$U\frac{\partial V}{\partial X} + V\frac{\partial V}{\partial Y} + W\frac{\partial V}{\partial Z} = -\frac{\partial P}{\partial Y} + \frac{1}{Re}\nabla^2 V \tag{3}$$

$$U\frac{\partial W}{\partial X} + V\frac{\partial W}{\partial Y} + W\frac{\partial W}{\partial Z} = -\frac{\partial P}{\partial Z} + \frac{1}{Re}\nabla^2 W \tag{4}$$

$$U\frac{\partial T}{\partial X} + V\frac{\partial T}{\partial Y} + W\frac{\partial T}{\partial Z} = \frac{1}{Re\,Pr}\nabla^2 T \tag{5}$$

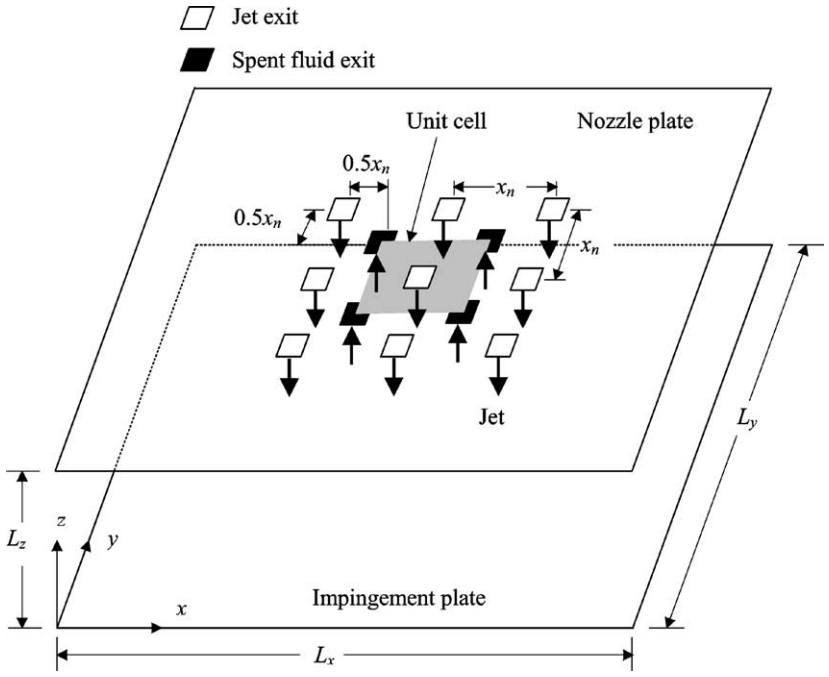

Fig. 1. Definitions of geometric parameters and the coordinate system.

The outlet boundaries are located far enough downstream for conditions to be substantially developed, accordingly the first derivative of all variables is set to zero at the outlet boundary. No slip boundary condition is used for the top and bottom solid walls except the W velocity at the jets and spent exit cross sections at the top wall. At the jet exit a uniform velocity profile is used, where the W velocity is set to be equal to one. Forced suction spent fluid exit is considered in this study and the spent fluid suction rate applied on the top plate is taken to be equal to jet flow rate.

Adiabatic boundary conditions are imposed on the top wall, except at the nozzles exit cross section where it was set to be equal to that of ambient. At the spent air exits the first derivative of temperature is set to zero. The bottom wall is set to a higher temperature than the ambient.

3. Method of solution

The governing equations are discretized by using the finite volume method in staggered, nonuniform grids. The grids are generated such that denser grid clustering is obtained around the nozzles and the spent fluid removal exits. In the z-direction a sine function distribution is employed, yielding denser grids near the top and near the impingement plate. A grid independence test has been made for $Re = 300$, $A_z = 1$, and $X_n = 5$ in order to determine the effect of number of grids on the local Nusselt number along a line joining the jet centers (Fig. 2(a)) and along a line above which the spent air exit holes are located (Fig. 2(b)). Along the line joining the jet centers the maximum difference between the results obtained by using $201 \times 201 \times 51$ and $161 \times 161 \times 39$

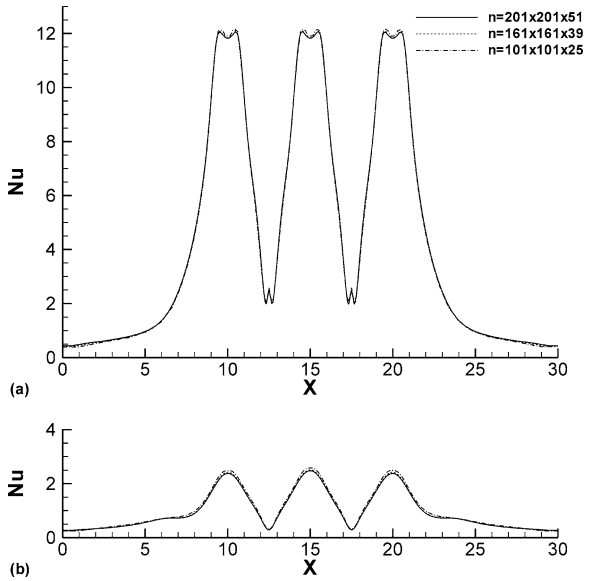

Fig. 2. Grid independence test for local Nusselt number at (a) $Y = 15$, and (b) $Y = 12.5$.

grids is 0.2%. The difference between $161 \times 161 \times 39$ and $101 \times 101 \times 25$ grids is 0.6%. For the Nusselt number along a line above which the spent air exit holes are located the corresponding differences are 1.1 and 2.9%. Hence, the $161 \times 161 \times 39$ grid system is used for all runs. The lengths of the nozzle plate and the impingement surface are taken of sufficient size in x- and y-directions ($L_x = L_y = 30D$) in order to eliminate end effects, and are open to atmosphere on all four sides. QUICK scheme (Leonard [10]) with ULTRA-SHARP flux limiting strategy (Leonard and Mokhtari [11]) was used to calculate the convection of a scalar term (ϕ)

at a control volume face. The extra neighboring points resulting from the application of QUICK scheme is written as the sum of the upwind face value plus a correction term involving the values from the previous iteration. The correction term is added to the source term in accordance with deferred correction procedure so that the numerical stability is increased, while keeping the seven diagonal structure of the coefficient matrix. The SIP method (Stone [12]), which is extended here to handle three-dimensional problems, is used to solve the momentum equations. The Conjugate gradient method is used to solve the pressure correction equation. The coefficient matrix resulting from the discretization of the energy equation is nonsymmetric and is solved using the Bi-CGSTAB (Van der Vorst [13]) iterative method. SSOR preconditioning is applied to the above iterative methods. The velocities are coupled with pressure terms using the SIMPLEC algorithm. An under relaxation factor of 0.7 for $Re = 100$–200 and 0.5 for $Re = 300$, 400 and 500 is used for momentum and energy equations in all calculations. Iterations are continued until the second norm of the residuals for all equations are reduced below 10^{-6}, where no significant variations of U, V, W or P are observed at this residual level. In the absence of experimental data under identical conditions the validation of the numerical code was performed against the experimental measurements of Sparrow and Wong [14], who used a developed slot-jet flow impinging on a naphthalene plate. The results are presented in Fig. 3 which depicts the variation of Nu with X. The full line represents the calculations with fully developed parabolic jet-inlet velocity profile using a slot jet of width equal L_y in y-direction. The symbols correspond to the experimental measurements. The agreement between the numerical results and the experimental measurements is in general good.

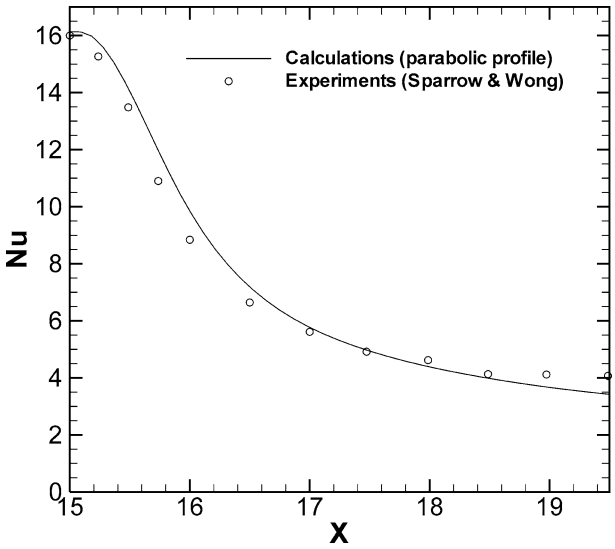

Fig. 3. Comparison of the local Nusselt number with experimental data for an slot jet ($Re = 450$, $A_z = 2$).

4. Results and discussions

Air is used as the working fluid, having a Prandtl number of 0.71. The analysis is performed for Reynolds numbers between 100 and 500 and aspect ratios, $A_z = L_z/D$, between 0.25 and 2. Center-to-center distance values between the jets are varied between $2D$ and $8D$. The cross section of the nozzles and the spent air exit holes is taken to be square and the velocity distribution at the exit of the nozzles and the spent air holes is assumed to have a flat profile. The velocity at the spent fluid exit is taken to be equal to the jet velocity at the nozzle exit.

The local convection heat transfer coefficient is defined as

$$h = \frac{q''_w}{t_w - t_j} \tag{6}$$

and the local Nusselt number is defined in terms of the jet width, D, as

$$Nu = \frac{h\,D}{k} \tag{7}$$

where it is also equal to the nondimensional heat flux and calculated from $Nu = \partial T/\partial Z|_{Z=0}$. Three-dimensional plot of the local Nusselt number for $Re = 500$, $X_n = 5$ and $A_z = 1$ is shown in Fig. 4. The jet stagnation areas are clearly distinguishable as local high Nusselt number regions. There is a small jump in heat transfer at the mid point between the jets. This is a result of the formation of upwash fountain created by the colliding wall jets after impingement. The magnitude of the Nusselt number at the center between the jets associated with the interaction between the opposing wall jets is expected to increase more when Reynolds number is

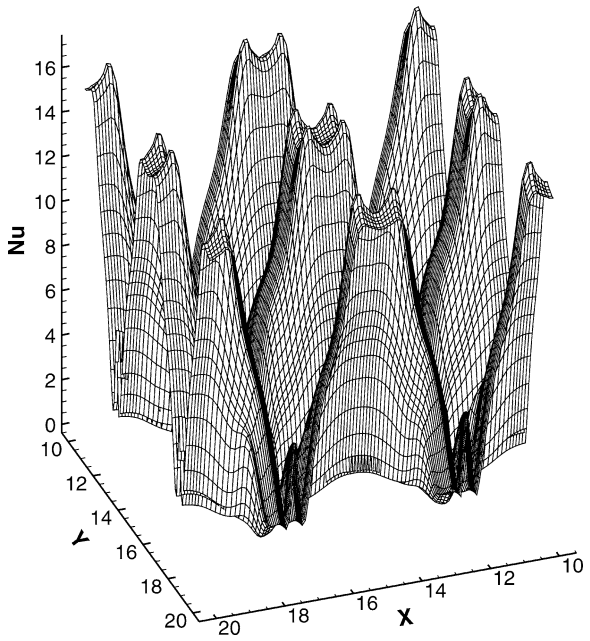

Fig. 4. The three-dimensional plot of the Nusselt number for $Re = 500$, $A_z = 1$, and $X_n = 5$ in the presence of spent air removal.

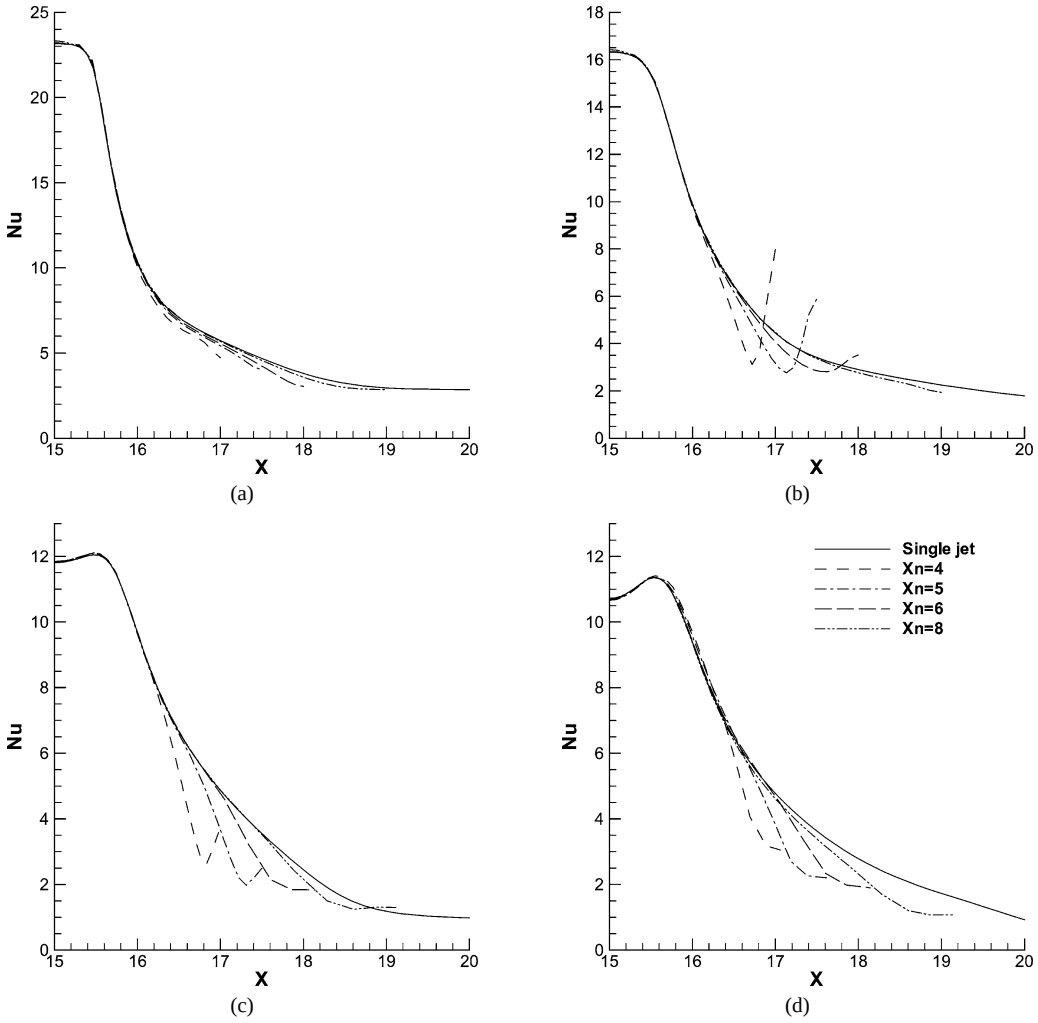

Fig. 5. Effect of jet-to-jet spacing on Nusselt number variation with spent air removal for $Re = 300$ and (a) $A_z = 0.25$, (b) $A_z = 0.5$, (c) $A_z = 1$, and (d) $A_z = 2$.

increased further. In fact measurements by Slayzak et al. [15] indicate that the local convection coefficients in the interaction zone can be comparable to those associated with the jet impingement regions for turbulent jets. The four off-center peaks of the Nusselt number for each jet are consistent with the jet velocity profile (not shown), which indicate that the jet velocity distribution plays a significant role in impingement cooling. The off-center peaks of the velocity and Nusselt number have also been observed in laminar rectangular single jet flows with small wall to jet distances (Sezai and Mohamad [16]). For turbulent jet cooling using round nozzles prior researchers have shown the presence of a secondary peak of local Nusselt number around the stagnation point in addition to the inner off-center peak. The inner peak which occurs at $r/D \approx 0.25$, where r is the radial distance from the stagnation point, is attributed to both the fluid acceleration out of the stagnation region which thins the local boundary layer and the influence of shear generated turbulence (Huber and Viskanta [5]). The presence of a single off-center peak of the Nusselt number in the present laminar study precludes the role of turbulence on the formation of this peak. The outer secondary peak was attributed to the result of transition to turbulent flow in the boundary layer (Ouden and Hoogendoorn [17] and Lytle and Webb [18]). Thus, for the rather low Reynolds numbers investigated in the present paper the formation of the outer peak in local Nusselt number is not expected. In fact, the secondary peak in Nusselt number for small nozzle to plate distances, mentioned by Huber and Viskanta [5] on a 3×3 square turbulent jet array and for single turbulent jet by Lytle and Webb [19] and Oyakawa et al. [20], is not found for the rather low Reynolds numbers investigated in this paper. As a result the heat transfer decreases rather smoothly away from the stagnation point. Moreover, no off-center peaks of the Nusselt number are observed for the rather small nozzle to plate distance of $L_z = 0.25D$. At this small nozzle to plate distance the local Nusselt number decreases abruptly in the locality below the spent air exit holes. The reduction of local Nusselt number is a result of detachment of wall jet from the impingement plate, where air flows vertically toward the spent air exit holes.

The effect of jet-to-jet spacing on the variation of local Nusselt number along x-direction at the mid section is shown in Fig. 5 for different separation distances between

the impingement plate and the confining jet nozzle plate. It is observed that the magnitude of the maximum Nusselt number is not affected by the jet-to-jet spacing, which may not be the case for turbulent jets. Huber and Viskanta [5], in their research on turbulent jet arrays, found that the local Nusselt numbers for $X_n = 8$ are larger in magnitude than those obtained for $X_n = 6$ and $X_n = 4$ for $A_z = 1$ and 6. The results of the present study shows that in the laminar range the magnitude of the local Nusselt number at the stagnation point is the same for a single jet and for a jet in an array due to negligible cross-flow effects for $X_n \geqslant 4$. For $A_z = 0.5$ and 1 (Fig. 5(b) and (c)) there is a sudden jump in Nusselt number at the localities corresponding to the midpoint between the jets. This is a result of the formation of upwash fountain created by the colliding wall jets after impingement. No such effect is observed for $A_z > 1$ values at $Re = 300$. However, the sudden jump in Nu at the collision point between the jets may also form at higher Reynolds numbers as seen earlier in Fig. 4. At a distance one-jet width downstream from the center of the jet, the magnitude of the Nusselt number of a single jet differs from that of a jet in an array for a jet-to-plate distance of $2D$ (Fig. 5(d)). The influence of the adjacent jet interference increases at lower jet-to-jet spacings, which is reflected by a reduction of Nusselt number for lower X_n values. Fig. 6 shows the effect of spent air removal on the variation of local Nusselt number along x-direction at the mid section for the central jet for $A_z = 1$. It is observed that the magnitude of the local Nusselt number around the jet stagnation point is not affected by the spent air removal. The heat transfer decreases steeper away from the stagnation points with the existence of the spent air removal compared with the cases of no spent air removal. A similar behavior has been observed in the experimental study of Huber and Viskanta [5] for turbulent jets for the same A_z value of 1, where the presence of spent air exits have no observable effect on the Nusselt number distribution. They have reported that Nusselt number increases in the presence of spent fluid exit holes when A_z is decreased down to 0.25. No such behavior is observed in this study for the laminar jet array system for $A_z = 0.25$. However, for a larger value of $A_z = 2.0$ the spent fluid removal increases the heat transfer rate as shown in Fig. 7. The effect of the spent air exits on Nusselt number distribution is greater for $X_n = 2.5$ as compared to $X_n = 3.0$. For $X_n = 2.5$, the closer jet spacing causes larger flow restrictions and adjacent jet interactions, which causes higher cross-flow effects between the jets. As a result, the difference between the distributions with and without spent air exits is larger for $X_n = 2.5$ than for $X_n = 3.0$. No steady solution could be obtained for lower X_n values for the same A_z and Re. It should be mentioned that the presence of spent air exits has been found to have no observable effect on the local Nusselt number distribution for A_z different than 2 in the Reynolds number range investigated in this study.

In an array with spent air exits, the Nusselt number averaged over the unit cell, (Fig. 1), represents the average of the entire array. Therefore, the local Nusselt number values were averaged over the unit cell defined by the central jet. Fig. 8 shows the comparison of the average Nusselt number values for the unit cell for different nozzle spacings for $A_z = 2$. For a given Reynolds number and A_z the average Nusselt number for $X_n = 4$ are larger than $X_n = 5$ and 8. This is expected because the jet array with $X_n = 4$ have the smallest unit surface area and larger mass flow rate compared with $X_n = 5$ and 8. This means that, while the unit surface area for $X_n = 8$ is covered by one impinging jet, an equivalent area for jet-to-jet spacing 4 is covered by four impinging jets and thus four times the mass flow rate of air for the same Reynolds number. The average Nusselt number with no spent air removal is higher than with spent

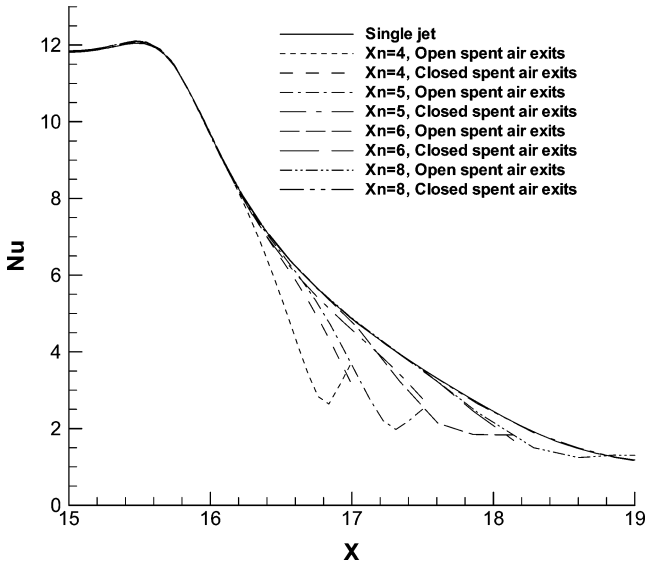

Fig. 6. Effect of spent air removal on local Nusselt number variation for $Re = 300$ and $A_z = 1$.

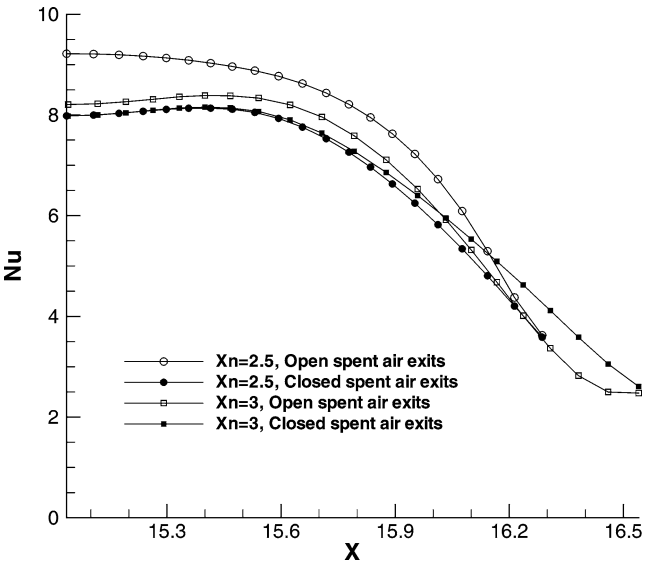

Fig. 7. Effect of spent air removal on local Nusselt number variation for $Re = 150$ and $A_z = 2$.

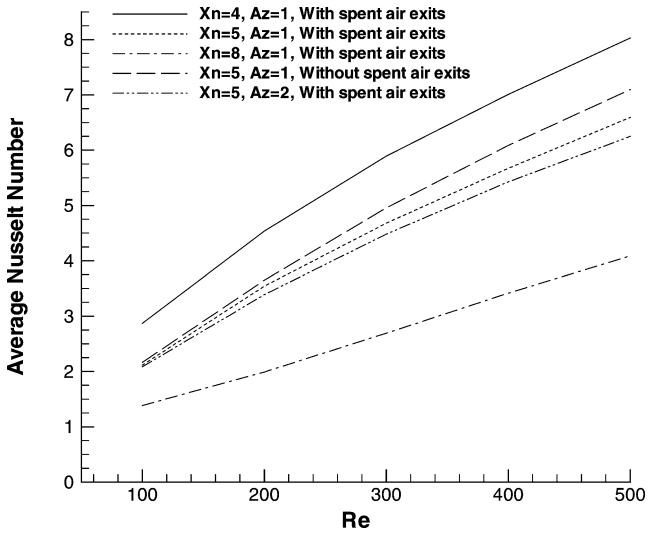

Fig. 8. Variation of average Nusselt number with Reynolds number for different X_n and A_z values.

air removal for a given X_n and A_z, which may not be the case for turbulent jets as found by Huber and Viskanta [5]. In addition there is also a considerable enhancement of the average Nusselt number when the separation distance between the jet and the plate is decreased.

5. Conclusions

Three-dimensional numerical simulations have been performed to gain understanding of the physical mechanisms which affect the variation of heat transfer in jet arrays with spent fluid removal from holes located between the jets on the nozzle plate.

For low nozzle to plate spacings $A_z \approx 0.25$ spent air removal has been found to lower the local Nusselt number in a region on the impingement plate below the spent air exit holes. This reduction is a result of detachment of the wall jet from the impingement plate as air flows upwards, towards the spent air exit holes.

It has been found that jet-to-jet spacing has no effect on the stagnation Nusselt number for $X_n \geqslant 4$ in the Reynolds number range investigated and that spent air removal cause a slight reduction in the local Nusselt number away from the stagnation point.

In the laminar range spent fluid removal increase the heat transfer rate for a nozzle to plate spacing of $2D$, which is in contrast with turbulent jet arrays, where spent fluid removal was reported to be effective for $L_z/D \leqslant 0.25$. The effect of spent air removal on the Nusselt number is greater for smaller jet-to-jet spacings due to larger flow restrictions and adjacent jet interactions. Spent air removal has almost no effect on the heat transfer rate for $X_n \geqslant 4$. Average Nusselt number is higher for lower jet-to-jet spacings due to higher mass flow rates on the unit surface area.

References

[1] L.W. Florschuetz, R.A. Berry, D.E. Metzger, Periodic streamwise variations of heat transfer coefficients for inline and staggered arrays of circular jets with crossflow of spent air, ASME J. Heat Transfer 102 (1980) 132–137.
[2] N.T. Obot, T.A. Trabold, Impingement heat transfer within arrays of circular jets: Part 1—Effects of minimum intermediate, and complete crossflow for small and large spacings, ASME J. Heat Transfer 109 (1987) 872–879.
[3] K. Garrett, B.W. Webb, The effect of drainage configuration on heat transfer under an impinging liquid jet array, ASME J. Heat Transfer 121 (1999) 803–810.
[4] B.R. Hollworth, L. Dagan, Arrays of impinging jets with spent fluid removal through vent holes on the target surface, Part 1: Average heat transfer, J. Engrg. Power 102 (1980) 994–999.
[5] A.M. Huber, R. Viskanta, Effect of jet–jet spacing on convective heat transfer to confined, impinging arrays of axisymmetric air jets, Internat. J. Heat Mass Transfer 37 (18) (1994) 2859–2869.
[6] P.Y. Tzeng, C.Y. Soong, C.D. Hsieh, Numerical investigation of heat transfer under confined impinging turbulent slot jets, Numer. Heat Transfer A 35 (1999) 903–924.
[7] S. Mikhail, S.M. Morcos, M.M.M. Abou-Ellail, W.S. Ghaiy, Numerical prediction of flow field and heat transfer from a row of laminar slot jets impinging on a flat plate, in: Proc. 7th International Heat Transfer Conf., Munchen, vol. 3, 1982, pp. 377–382.
[8] S.H. Seyedein, M. Hasan, A.S. Mujumdar, Laminar flow and heat transfer from multiple impinging slot jets with an inclined confinement surface, ASME J. Heat Transfer 37 (13) (1994) 1867–1875.
[9] H. Laschefski, T. Cziesla, G. Biswas, N.K. Mitra, Numerical investigation of heat transfer by rows of rectangular impinging jets, Numer. Heat Transfer A 30 (1996) 87–101.
[10] B.P. Leonard, A stable and accurate convective modelling procedure based on quadratic upstream interpolation, Comput. Method Appl. Mech. Engng. 19 (1979) 59–98.
[11] B.P. Leonard, S. Mokhtari, Beyond first order upwinding: the ULTRA–SHARP alternative for nonoscillatory steady-state simulation of convection, Internat. J. Numer. Methods Engrg. 30 (1990) 729–766.
[12] H.L. Stone, Iterative solution of implicit approximations of multidimensional partial differential equations, SIAM J. Numer. Anal. 5 (1968) 530–558.
[13] H.A.V. Van der Vorst, BICGSTAB: A fast and smoothly converging variant of Bi-CG for the solution of non-symmetric linear systems, SIAM J. Sci. Statist. Comput. 10 (1989) 1174–1185.
[14] E.M. Sparrow, T.C. Wong, Impingement transfer coefficients due to initially laminar slot jets, Internat. J. Heat Mass Transfer 18 (1975) 597–605.
[15] S.J. Slayzak, R. Viskanta, F.P. Incropera, Effect of interaction between adjacent free surface planar jets on local heat transfer from the impingement surface, Internat. J. Heat Mass Transfer 37 (2) (1994) 269–282.
[16] I. Sezai, A.A. Mohamad, 3-D simulation of laminar rectangular impinging jets, flow structure and heat transfer, ASME J. Heat Transfer 121 (1999) 50–56.
[17] C.D. Ouden, C.J. Hoogendoorn, Local convective heat transfer coefficients for jets impinging on a plate: experiments using a liquid crystal technique, in: Proc. of the 5th Heat Transfer Conf., AICHE, New York, vol. 5, 1974, pp. 293–297.
[18] D. Lytle, B.W. Webb, Secondary heat transfer maxima for air jet impingement at low nozzle-to-plate spacing, in: Experiment Heat Transfer, Fluid Mechanics and Thermodynamics, New York, 1991, pp. 776–783.
[19] D. Lytle, B.W. Webb, Air jet impingement heat transfer at low Nozzle-plate spacings, Internat. J. Heat Mass Transfer 37 (1994) 1687–1697.
[20] K. Oyakawa, S. Matsuda, M. Yaga, Study on impingement heat transfer with non-circular jets using infrared imaging method, in: Proc. of the 4th World Conf. on Experiment Heat Transfer, Fluid Mechanics and Thermodynamics, Brassels, 1997, pp. 1807–1814.